PFC/JA-94-31

Detached Scrape-off Layer Tokamak Plasmas

J. Kesner

February 1995

MIT Plasma Fusion Center
Cambridge, Massachusetts 02139 USA

This work was supported by the US Department of Energy under contract DE-FG02-91ER-54109.

Submitted for publication in: Physics of Plasmas

Detached Scrape-off Layer Tokamak Plasmas

J. Kesner

Plasma Fusion Center

Massachusetts Institute of Technology

Cambridge, Massachusetts 02139

Cambridge, Massachusetts

ABSTRACT

The equilibrium and stability of scrape-off layer plasmas are considered using a 1-dimensional treatment of coupled heat conduction and pressure balance equations. It is found that, for sufficiently low temperature and high neutral density, a region of greatly reduced power flux to the end plate can be achieved. The plasma in the vicinity of the end wall is characterized by a sharp plasma pressure gradient and a relatively low temperature, $1 < T_0 < 10$ eV.

PACS 52.40.Hf, 52.55.Fa

I. Introduction

Diverted tokamak experiments have observed a phenomenon known as detachment. For a sufficiently strong gas feed at the plasma edge the plasma pressure at the end wall has been observed in experiments to drop more than an order of magnitude and the temperature will fall into the range of 1 to 5 eV [1-3]. Additionally they observe a greatly reduced heat flux to the divertor end plate. For a fusing plasma the ability to absorb the high levels of heat flux that are expected to appear at the divertor plate is problematical and this phenomenon may be important in tokamak reactor applications.

A sharp reduction of the temperature and pressure[4-6] has been predicted to occur at the end wall of a diverted tokamak. Stangeby[6] has shown that the dominance of charge exchange over ionization at low temperatures can result in the formation of a sharp pressure gradient at the end plate. It has also been shown [7] that the continuity and pressure balance equations predict a bifurcation in the location of the ionization front.

In this study we show that detached solutions result from the simultaneous solution of the heat conduction and the pressure balance equations. We permit the pressure to fall in the vicinity of the end plate and define detachment as the point where the plasma pressure at the wall drops to below an order of magnitude of its upstream value. This transition occurs for a sufficient level of neutral density. The simultaneous solution of the heat conduction and pressure balance equations locates the ionization front near to the end plate. More specifically we observe that before detachment the ionization front will move away from the end plate as the neutral density increases while after detachment increasing neutral density will cause the ionization front to move back towards the end plate. The radiation zone encompasses the region in which impurities are present and is expected to extend out from the ionization front to the vicinity of the x-point.

II. Scrape-off-layer Model

We will use fluid equations[8] for temperature (T), pressure (p) and fluid flow (Γ=nu), with $n = (n_e + n_i)/2$ and T=$(n_e T_e + n_i T_i)/2n$ and assume subsonic flow. MKS units with temperatures in eV are used throughout. The parallel thermal conductivity is taken to be $\kappa_{\|} = (7/2)c_{\|}T_e^{5/2}$ with $c_{\|} = 800\ Wm^{-1}eV^{-7/2}$ and we define a temperature-like variable $\xi \equiv T^{7/2}$. We will examine the equilibria of the following equations:

$$c_{\|}\frac{\partial^2 \xi}{\partial s^2} = P_{rad}(\xi) - h(s) \tag{1a}$$

$$\frac{\partial p}{\partial s} = m_i n_N \Gamma \langle \sigma v \rangle_{CX} \tag{1b}$$

$$\frac{\partial \Gamma}{\partial s} = n_e n_N \langle \sigma v \rangle_i. \tag{1c}$$

Eq. (1a) is the heat conduction equation and Eq. (1b) the parallel pressure balance, s is the along-the-field line distance and $p = 2nT$. $P_{rad}(\xi)$ includes heat loss due to radiation, ionization and charge-exchange, and $h(s)$ the heat per unit volume entering the scrape-off layer flux tube. Eq. (1b) is a simplified parallel force balance equation and assumes subsonic flow velocity [7] and sufficiently long charge-exchange, elastic scatter and ionization mean free paths so that charge exchanged neutrals can escape from the plasma and deposit their momentum on the divertor chamber walls[6] (This assumption is discussed further in Sec III). $\langle \sigma v \rangle_{CX}$ is the sum of the rate coefficients for charge exchange and elastic scatter and $\langle \sigma v \rangle_i$ is the ionization rate coefficient.

We consider a simple geometry for the scrape-off layer with a recycle region that includes a region in which ion-neutral interactions are dominated by charge exchange and elastic collisions (the CX/EC region) followed by an ionization region. The recycle region is followed by a heating region. The CX/EC region extends from the divertor plate at s=0 out to $s = \Delta$, the ionization region extends from $s = \Delta$ to the vicinity of the x-point at $s = L_x$ and the heating region extends from L_x to the symmetry point at $s = L$. In

the CX/EC region ($0 < s < \Delta$) the neutral density is taken to be a constant, n_N. In the ionization region ($\Delta < s < L_x$) charge exchange is unimportant. In the heating region ($L_x < s < L$) we impose a uniform heat source which represents the power flow across the separatrix and into the scrape-off layer.

Charge exchange can add to P_{rad} in Eq. (1a). Normally the charge-exchange power loss, $P_{CX} = 1.5nn_N\langle\sigma v\rangle_{CX}(T_i - T_{FC})$ with T_i the ion temperature and T_{FC} the Franck-Condon neutral temperature. This term is clearly small at low n_N and it is also small for high n_N since in this limit $T_i \rightarrow T_{FC}$. (The ion temperature T_i approaches T_{FC} when charge-exchange cooling dominates electron-ion equilibration, i.e. when $n_N > 1/(\langle\sigma v\rangle_{CX}\tau_{eq}$ with $\tau_{eq} = 3.1 \times 10^{14}\mu T^{3/2}/nln(\Lambda)$ and $\mu \equiv m_i/m_H$, the ion mass normalized to the hydrogenic mass. In the range of interest $\tau_{eq} \sim 1 \times 10^{-5}$ sec and $\langle\sigma v\rangle_{CX} = 4 \times 10^{-14}\ m^3/s$ and therefore for $n_N > 2.5 \times 10^{18}\ m^{-3}$ the charge exchange cooling term becomes unimportant).

We apply the sheath boundary condition at s=0 and thus the boundary conditions are

$$\xi'(0) = c_0\gamma_s p_0\xi^{1/7}(0),\ \xi'(L) = 0,\ p(L) = p_1,\ \Gamma(L_x) = 0 \tag{2}$$

with γ_s is the sheath heat transfer coefficient and the constant, $c_0 = (e^{3/2}/c_\parallel)\sqrt{1/2m_i}$ with e the electron charge.

We will further simplify equations (1a)-(1c) in the following ways:

1. We assume a constant volumetric heating beyond the x-point, i.e. $h(s) = h_0H(s-L_x)$ with $H(x)$ the heavyside function, i.e. $H(x)$=0 for $x < 0$ and $H(x)$=1 for $x > 0$. In calculations the heavyside function is approximated by $0.5[1 + tanh(\alpha(s - s_0))]$ with $\alpha = 2$ to 5.

2. Utilizing the observation that for $T < T_{CX}$ with $T_{CX} \sim 10$ eV many charge exchange events occur per ionization[6] we approximate $\langle\sigma v\rangle_{CX} = S_{CX}H(T_{CX} - T)$ and $\langle\sigma v\rangle_i = S_iH(T - T_{CX})$ with $S_{CX} = S_i = 4 \times 10^{-14}\ m^3/s$. This approximation maintains the important physics associated with the qualitative change in the neutral-ion interaction

that occurs at low temperatures and it decouples the continuity equation, Eq. (1c), from equations (1a) and (1b). We define the boundary, Δ, of the CX/EC region by $T(\Delta) = T_{CX}$.

3. We have considered two forms for the radiation function:

- A local thermodynamic equilibrium (LTE) form

$$P_{rad}(T) = n_e n_C L_0 \frac{T^3}{T^5 + T_{rad}^5}. \tag{3a}$$

n_C is the impurity density (i.e. Carbon) which is assumed to be constant and T_{rad} represents the temperature at the peak of the radiation curve, i.e. for Carbon in local thermodynamic equilibrium $T_{rad} = 8$ eV and $L_0 = 1.2 \times 10^{-31}\ Wm^{-3}$. In the appendix we will approximate Eq. (3a) by a δ-function.

- A non-local thermodynamic equilibrium form

$$P_{rad}(T) = 0.5 n_e n_C L_0 [1 + Tanh \frac{T - T_{rad}}{2}] H(L_x - s). \tag{3b}$$

For $T_{rad} = 5$ eV this radiation function rises to a plateau at $T \sim 10$ eV. In this approximation we also assume that the impurity radiation is localized below the x-point which is equivalent to assuming that impurities are localized to the divertor region.

With these approximations equations (1) become

$$c_{\parallel} \frac{\partial^2 \xi}{\partial s^2} = P_{rad} - h_0 H(s - L_x). \tag{4a}$$

$$\frac{\partial p}{\partial s} = m_i n_N \Gamma_0 S_{CX} H(T_{CX} - T). \tag{4b}$$

with boundary conditions from (2). The subscript 0 will denote quantities at the divertor plate (s=0) and 1 denotes the respective quantities at the symmetry point (s=L).

II. Solutions to Equilibrium Equations.

II A. Constant Pressure Along-the-Field-Line

For sufficiently low neutral density Eq. (4b) reduces to $p = constant = p_1$ and the heat conduction equation may be solved with a prescribed value for p. The boundary conditions on the heat conduction equations given by Eq. (2) will determine the temperature at the end plate and at the symmetry point.

We have solved these equations numerically with parameters that are typical of the C-mod experiments[9], L=12 m, $L_x = 2m$, $p_1 > 100$ Pa. We will use the non-LTE radiation function from Eq (3b) and note that solutions that utilized the radiation function from Eq. (3a) did not differ substantially. The width of the scrape-off layer, λ, enters the determination of the input power density, $h_0 = P_{sol}/(A_{sep}\lambda)$ with P_{sol} the total heat entering the scrape-off layer and we use for λ an experimentally determined value of the pressure scale length[9]

$$\lambda = \frac{0.3}{T_1}$$

with T_1 the symmetry point temperature in eV. Fig 1 shows temperature profiles for three values of upstream pressure. For $p_1 = 192$ Pa we find that at the divertor plate T(0)=10 eV whereas for a higher upstream pressure, $p_1 = 480$ Pa, we obtain T(0)= 0.1 eV. When the temperature at the end plate is small, i.e. $T(0) << 1$ eV, the plasma does not conduct appreciable heat to the end plate and it arguably can detach. (Notice we have not reduced the temperature to zero which would eliminate the class of solutions in which we are interested). Fig. 1 also shows a "detached" solution, obtained for $p_1 = 512$ Pa in which we have allowed the plasma to be located 0.5 m from the end plate leaving a region of near zero temperature in the vicinity of the end plate. A similar result has been shown by Hutchinson[10].

We have analysed the stability of these equilibria. We perturb Eq. (4) ($\xi \rightarrow \xi + \delta\xi$) and obtain for $\delta\xi$

$$\gamma\delta\xi = c_{\parallel}\frac{\partial^2\delta\xi}{\partial s^2} - n_e n_C \frac{dL}{d\xi}\delta\xi + \left[\frac{dh_0}{d\xi}\delta\xi\right]_L \tag{7a}$$

with γ the growth rate. The boundary conditions on $\delta\xi$ are

$$\frac{\partial\delta\xi}{\partial s}(0) = \frac{\gamma_s p_0}{7\xi^{6/7}}\delta\xi(0), \quad \frac{\partial\delta\xi}{\partial s}(L) = 0. \tag{7b}$$

We can solve Eq. (7) consistently with the equilibrium equation (Eq 4a) to evaluate stability. To solve we set $\gamma = 0$ and integrate Eq. (7a) from the end plate (s=0) to the symmetry point (s=L) with an arbitrary amplitude for $\delta\xi(0)$ and an initial slope given by Eq. (7b). Note that $\partial\delta\xi(0)/\partial s > 0$. Since the boundary condition at the symmetry point is $\partial\delta\xi(L)/\partial s = 0$ we can show that the solutions are stable if no extrema occur before the location of the symmetry point, i.e. if $\partial\delta\xi(s)/\partial s > 0$ for $0 < s < L$. Fig 2 shows the perturbation $\delta\xi$ for the equilibrium having $p_1 = 480$ Pa that is shown in Fig 1. We observe that for $\gamma = 0$ no maxima is observed in the range $0 < s < 15$ m and one can show that a negative γ value is required to satisfy the boundary condition $\partial\delta\xi(L)/\partial s = 0$. In this way we find that all of the equilibria shown in Fig. 1 are stable.

To understand better the calculated stability of these solutions we can formulate a quadratic form by multiplying by $\delta\xi$ and integrating along the length of the field line:

$$\gamma = \frac{-\int_0^L [c_{\parallel}\delta\xi_s^2 + n_e n_C \frac{dL}{d\xi}\delta\xi^2]ds - g\delta\xi^2(0)}{\int_0^L \delta\xi^2 ds} \tag{8}$$

with $\delta\xi_s \equiv \partial\delta\xi/\partial s$ and g=$\gamma_s p_0/(7\xi^{6/7})$. Eq. (8) indicates that parallel conductivity is stabilizing, the radiation function can be stabilizing or destabilizing depending on whether the slope is respectively positive or negative (for the non-local-thermodynamic-equilibrium function of Eq. (3b) it is stabilizing) and the boundary condition adds a term that is always stabilizing. The boundary term stabilization comes about because as the temperature at the end plate rises the outflow of heat increases (and visa versa), which tends to damp

the temperature rise. When $T(0) \gtrsim 5$ eV this term can be dominant. For T(0) $\lesssim 1$ eV the stabilization of the boundary term becomes small but for the non-LTE radiation function the the radiation term is stabilizing while the LTE form has a cancellation between regions of positive and negative slope.

In experiments the pressure is observed to drop dramatically with detachment[9] and the temperature remains in the 1 to 8 eV range. Therefore the constant pressure model differs from experimental observations in the pressure and temperature dependences. In the next section we consider the case of non-uniform pressure.

II B. Pressure Variation Along-the-Field-Line

We now consider the solution of the equilibrium equations (4a,4b) for significant neutral pressure. In solving this set of equations we fix the upstream plasma pressure, p_1 to be similar to the measured value (this is the boundary condition for the pressure balance equation) and vary the pressure gradient, p_0'. The pressure gradient p_0', is a measure of neutral density,

$$n_N \approx \frac{p_0'}{m_i \Gamma_0 \langle \sigma v \rangle_{CX}}$$

and $\Gamma_0 = c_{s0} n_0$ with c_{s0} the sonic speed at the end plate, $c_{s0} = \sqrt{2T_0/m_i}$. Table I lists the results of four such calculations in which we have fixed L=12 m, $L_x = 2$ m, $p_1 = 480$ Pa, $T_{CX} = 10$ eV and use the non-LTE radiation function (Eq. 3b) with $n_C = 10^{18}\ m^{-3}$.

Fig 3a displays the temperature profiles in the divertor region ($0 < s < L_x$) for calculations in which we assume high (solid curve) and low (dashed curve) respective neutral densities (cases III and II in Table I). Fig 3b displays the pressure profiles for these two cases. Notice that for case II the temperature drops to near zero while the pressure remains high whereas for the detached case III the pressure at the end plate is near zero while the temperature is ~ 4 eV. Fig 3c shows the corresponding density profiles. In the detached case (III) the plasma density falls in the vicinity of the plate because of the drop in pressure (n=p/2T).

The decrease in both the density and temperature at the divertor plate indicates a reduced mass flow of plasma into the divertor plate (due to the sonic boundary condition) and results in a reduction in the source of recycled neutrals. In steady state the reduction of the plasma outflow to the divertor plate must be consistent with a reduction of the ionization source along the field line. (We have assumed that mass flow from the core plasma into the scrape-off layeris negligible compared with re-ionization of recycled neutrals). This requires that detachment be accompanied by a reduced level of neutral density in the ionizing region. The ionization source does not enter our calculation but we could, in principle, use the continuity equation (Eq 1c) to determine an average neutral density in the ionization region. The neutral density in the ionization region can be substantially smaller that in the CX/EC region.

Fig 3d displays the radiated power in the vicinity of the end plate. The along-the-field-line radiation profiles are similar for the two cases shown. The peak of radiated power occurs near to the end wall because of the high density and low temperature in this region. (For a higher value of T_{rad} or a lower value of T_{CX} the radiation peak would occur further upstream). For the radiation model used there is substantial impurity radiation throughout the divertor region extending up to the x-point.

Fig 4 shows the ratio of upstream pressure to pressure at the divertor plate (p_1/p_0) as a function of the neutral atomic hydrogen density (m^{-3}) for several calculated equilibria. At low neutral density p_1/p_0 is near 1 and rises slowly with increasing neutral density. Above a critical value of neutral density, however, p_1/p_0 rises quickly to a large value characteristic of detachment, $p_1/p_0 \sim 10$. From Table I we observe that the divertor plate temperature can be higher in the detached state compared to the constant pressure, low heat flux equilibria. In the detached state the power flux at the end plate is reduced because of the large reduction in the plasma pressure.

The boundary between the CX/EC and ionizing regions was defined to be $T(\Delta) \sim$ 10 eV. Fig. 5 displays the position of the ionization front (Δ) vs the neutral hydrogen density. We observe that at low neutral density the ionization front is near the end plate, $\Delta/L_x \sim 0.2$ and after detachment ($p_1 >> p_0$) the ionization front will approach the end

plate as the neutral density increases. The movement of the boundary of the CX/EC region occurs because as the neutral density increases a larger pressure gradient can be balanced in a smaller region. Δ also serves as a measure of the peak of impurity radiation (Fig 3d) because of the combination of high density and relatively low temperatures at this location.

To analyse the stability of the non-constant-pressure equilibria we must perturb the pressure balance (4b) as well as the heat conduction equation (4a). Taking $p \rightarrow p + \delta p$ with the boundary condition $\delta p(0) = 0$ leads to the result

$$\delta p(s) = -p_0' H(s - \Delta) \left[\frac{\delta \xi}{d\xi/ds} \right]_{s=\Delta}.$$

The variation of δp will introduce an additional destabilizing term into Eq. (7a) which now becomes

$$\gamma \delta \xi = c_{\parallel} \frac{\partial^2 \delta \xi}{\partial s^2} - n_e n_C \frac{dL}{d\xi} \delta \xi + \left[\frac{dh_0}{d\xi} \delta \xi \right]_L - \frac{n_c L(\xi)}{\xi^{2/7}} \delta p. \tag{9}$$

We may observe from Fig 2 that the perturbation $\delta \xi$ is small near $s = \Delta$ in order to avoid the stabilizing portion of the radiation function. Therefore the corrections shown in Eq. (9) are usually not important and the equilibria shown in Table I were found to be stable.

III. Discussion

We have seen that the heat conduction equation coupled to a charge-exchange dominated parallel pressure balance equation can predict a sharp reduction in the heat flow to the divertor target plate. Recalling that the (conductive) heat flow to the target, $q_{wall} \propto p_0 \sqrt{T_0}$, it is clear that this reduction can be accomplished in two ways: by reduction of either the plasma temperature or the plasma pressure near the end plate. These two operating modes are obtained as follows:

i. For sufficiently low neutral density there is an approximate pressure balance along-the-field-line and in the presence of sufficient radiation the heat flux can be reduced when the plasma temperature at the end plate becomes sufficiently low. Typically $T_0 < 1$ eV is required for a substantial reduction of heat flow to the end plate for the constant pressure case. Because of the high particle flux to the end plate in this operating mode the energy of recombination (at the divertor plate) can add substantially to the total power absorbed by the end plate.

ii. For sufficiently high neutral density the pressure will fall in the vicinity of the end plate if the temperature is below the critical temperature for charge exchange and elastic collisions to dominate in the neutral-ion interaction. When pressure p_0 becomes small q_{wall} will likewise fall. Additionally the particle flux is lower (due to decreased recycle) which reduces the recombination energy deposited at the divertor plate.

The large pressure drop and the prediction of non-negligible target plate temperatures, $1 < T_0 < 10$ eV in mode (ii) is consistent with experimental observations.

The temperature at which charge-exchange dominates over ionization is set by atomic processes and even in a reactor size tokamak the temperature of the plasma stream flowing past the x-point must be relatively low for detachment to occur. If we only consider the scrape-off layer upstream of the x-point ($L_x < s < L$) and assume that radiation and neutral effects are unimportant in this region we can obtain from Eq. (4a)

$$\xi_L = \xi_x + \frac{P(L - L_x)^2}{4\pi\kappa a^2 A c_{\|} \lambda} \tag{10}$$

with P the power entering the scrape-off layer and A the aspect ratio. Taking $L = \pi a \kappa q$ with q the cylindrical safety factor and κ the scrape-off layer ellipticity and assuming $L >> L_x$ and $\xi_L >> \xi_x$ we can estimate the maximum temperature in the scrape-off layer

$$T_L = \left[\frac{\pi}{4}\frac{P q^2 \kappa}{c_{\|} A \lambda}\right]^{2/7} . \tag{10a}$$

Taking (C-mod parameters) $P = 0.4$ MW, A=3, $\kappa \sim 1.6$, $\lambda \sim 0.007$ m, and q=3, Eq.

(10a) gives T_L ~36 eV. For a reactor with $P = 400$ MW, we guess that $\lambda \sim 0.1$ m (the scaling of λ is not known) and taking similar q and aspect ratio we would obtain $T_L \sim 120$ eV. Thus we see that detachment requires that the temperature in the scrape-off layer be relatively cool. The density does not enter into Eq. (10a) and therefore elevating the edge density provides a means to obtain a cool edge temperature.

An important caveat is that in the pressure balance equation we have assumed that for efficient momentum transfer the charge-exchange products will leave the flux tube within a single mean-free-path[6]. Typically the mean-free-path for charge-exchange neutrals is ~ 1 cm. If the charge-exchanged neutral is re-ionized within the plasma the momentum will be transferred into the plasma at that location. Detachment is observed to first occur near the strike point at the separatrix[9] and if the charge exchange neutrals are re-ionized in warmer regions this can lead to partial detachment. In reactor-size devices it is desirable that the detached region be a substantial fraction of the scrape-off layer width. An accurate determination of the distance that a neutral will travel before being ionized would require a 3-dimensional calculation and is beyond the scope of this study.

It has been observed that consistent with continuity and pressure balance, (Eqs. (1b) and (1c)) two solutions for Δ are possible[7], one with the ionization front located near to the end plate and one near to the x-point. We have found, however, that the heat conduction equation will locate the ionization front relatively close to the end wall. Furthermore as neutral pressure increases the ionization front will move towards the end plate. This solution leaves a relatively large ionization region (of length $L_x - \Delta$) and can lead to high flow speeds. The analysis is further complicated if the flow becomes supersonic and we have assumed that this does not happen. The flow speed obtained depends on the level of neutral density in the ionization region ($\Delta < s < L_x$), which is typically lower than the neutral density nearer to the end plate. Solutions with $\Delta \lesssim L_x$ have been obtained but typically these solutions require $T_0 << 1$ and substantially lower upstream plasma pressure than is observed in experiments. Therefore we conclude that these solutions are probably not useful for tokamak design.

IV. Conclusions

A 1-dimensional detachment model based on charge exchange transfer of momentum agrees qualitatively with experimental results on several points:

- Above a critical neutral density the plasma pressure will drop a factor of >10 in the vicinity of the end plate provided the plasma temperature is sufficiently low.
- For a detached plasma the plasma temperature at the end plate can be in the range $1 < T_0 < T_{CX}$ with $T_{CX} < 10$ eV. The temperature in the vicinity of the x-point must be reduced to $\lesssim 30$ eV for detachment to occur.

Since the location of the radiation front within the divertor region is a function of the neutral pressure a sweeping of the power flux within the divertor region might be obtainable if the neutral pressure could be varied in a systematic way.

The radiation and charge exchange profiles are not uniform and may peak near to the ionization front. Additionally an x-point Marfe may accompany (or precede) detachment[11] and this would cause copious radiation from the vicinity of the x-point.

The requirement that a cool plasma enter the divertor region in order to obtain detachment imposes a severe restriction for reactor design. Furthermore for detachment to be useful the width of the detached zone must be comparable to the width of the SOL pressure profile. Nevertheless detachment may play an important role in the operation of a divertor in a tokamak based fusion reactor.

Acknowledgements

The author would like to acknowledge important discussions with P. Stangeby, B. LaBombard, B. Lipschultz, G.M. McCracken and J.P. Freidberg. This work was supported by the U.S. Department of Energy.

Appendix - Approximate Analytic Solution

Equations (4a) and (4b) can be solved analytically with a simplified radiation function. We will substitute for the radiation function a δ-function centered at T_{rad}, i.e.

$$P_{rad}(T) = R_0\delta(T - T_{rad}).$$

In the region adjoining the end plate ($0 < s < \Delta$) the heat conduction equation is

$$c_{\|}\frac{\partial^2\xi}{\partial s^2} = 0 \tag{11}$$

with the boundary condition $\xi_0' = c_0\gamma_s p_0\xi_0^{1/7}$. $\xi_0 \equiv \xi(0)$ and $c_0 = (e^{3/2}/c_{\|})\sqrt{1/2m_i}$. The solution of Eq. (11) yields

$$\xi = c_0\gamma_s p_0\xi_0^{1/7}s + \xi_0 \quad for\ 0 < s < \Delta_T. \tag{12}$$

Imposition of the requirement that $T(\Delta_T) = T_{rad}$ will determine Δ_T as a function of ξ_0 and p_0:

$$\Delta_T = \frac{T_{rad}^{7/2} - \xi_0}{c_0\gamma_s p_0\xi_0^{1/7}}. \tag{13}$$

Defining T_{cx} as the temperature at which charge-exchange and elastic collisions become the dominant neutral-ion interaction and Δ_p by $T(\Delta_p) = T_{CX}$ we can determine p_1 from $p_1 = p_0 + p_0'\Delta_p$. Thus:

$$p_1 = p_0 + m_i n_N \Gamma_0\langle\sigma v\rangle_{CX}\frac{T_{cx}^{7/2} - \xi_0}{c_0\gamma_s p_0\xi_0^{1/7}}. \tag{14}$$

In the region $\Delta_T < s < L_x$ we obtain from Eq. (11)

$$\xi(s) = \xi_0 + (c_0\gamma_s p_0\xi_0^{1/7} + \frac{R_0}{c_{\|}})s - \frac{R_0}{c_{\|}}\Delta_T \quad for\ \Delta_T < s < L_x. \tag{15}$$

In the region $L_x < s < L$ we must solve

$$c_{\|}\frac{\partial^2 \xi}{\partial s^2} = -h_0 \tag{16}$$

with the boundary condition $\xi'(L) = 0$. This yields

$$\xi = \xi_0 + \frac{h_0}{c_{\|}}(sL - \frac{s^2}{2} - LL_x + \frac{L_x^2}{2}) + \frac{R_0}{c_{\|}}(L_x - \Delta_T) + c_0\gamma_s p_0 \xi_0^{1/7} L_x \quad for\ L_x < s < L \tag{17}$$

and continuity of the derivative at $s = L_x$ yields the following relationship for ξ_0:

$$R_0 = h_0(L - L_x) - c_{\|}c_0\gamma_s p_0 \xi_0^{1/7}. \tag{18}$$

If we know the temperature parameter ξ_p at a point s_p we can combine Eq 17 and 18 to obtain h_0:

$$h_0 = c_{\|}\ \frac{\xi_p - \xi_0 - c_0\gamma_s p_0 \xi_0^{1/7}\Delta_T}{s_p L - \frac{s_p^2}{2} - \frac{L_x^2}{2} - \Delta_T(L - L_x)}. \tag{19}$$

Normally p_0, ξ_0, p_p, and ξ_p are measured with p_p and ξ_p the respective pressure and temperature parameter at a probe located in the scrape-off layer. Given p_0 and ξ_0 Eq (13) will determine Δ_T. Eq (14) will determine the implied neutral density from the measurement of p_2 (For $s > \Delta_p$ the pressure is constant so $p_2 = p_1$). Given the geometric quantities, L_s and L_x equations (18) and (19) determine the heating and power radiated from the scrape-off layer. Finally equations (12), (15) and (17) determine the temperature profile along the field line.

References:

[1] I.H. Hutchinson, R. Boivin, F. Bombarda, P. Bonoli, S. Fairfax, C. Fiore, J. Goetz, S. Golovato, R. Granetz, M. Greenwald, S. Horne, A. Hubbard, J. Irby, B. LaBombard, B. Lipschultz, E. Marmar, G.M. McCracken, M. Porkolab, J. Rice, J. Snipes, Y. Takase, J. Terry, S. Wolfe, C. Christensen, D. Garnier, M. Graf, T. Hsu, T. Luke, M. May, A. Nemczewski, G. Tinios, J. Schachter and J. Urban, Physics of Plasmas **1**, 1511 (1994).

[2] G. Janeschitz, S. Clement, N. Gottardi, M. Lesourd, J. Lingertat, C. Lowry, G. Radford, G. Saibene, M. Stamp, D. Summers, A. Taroni, P.R. Thomas, G. Vlases in *Proceedings of 19th European Conf on Controlled Fusion and Plasma Physics*, Innsbruck, 1992, (European Physical Society, Geneva, 1992), Vol 16C, Part II, 727.

[3] T.W. Petrie, D. Buchenauer, D.N. Hill, C. Klepper, S. Allen, R. Campbell, A. Futch, R. Groebner, A. Leonard, S. Lippmann, M. Mahdavi, M. Rensink and W. West, J. Nucl. Mater. **196-198**, (1992) 848.

[4] S.I. Krasheninnikov, A.S. Kukushkin, V.I. Pistunovich and V.A. Pozharov, Nucl. Fus, **27**, 1805 (1987).

[5] K. Borrass, P.C. Stangeby, in *Proceedings of 20th European Conf on Controlled Fusion and Plasma Physics*, Lisbon, 1993, (European Physical Society , Geneva, 1993), Vol 17C, Part II, 763.

[6] P.C. Stangeby, Nucl. Fus, **33**, 1695 (1993).

[7] Ph. Ghendrih, "Bifurcation to a Marfing Divertor Plasma Governed by Charge Exchange", submitted to Phys. Plasmas (1994).

[8] S.I. Braginskii, in *Reviews of Plasma Physics*, edited by M.A. Leontovich (Consultants Bureau, New York, 1965) Vol. I, p. 205.

[9] B. LaBombard, D. Jablonski, B. Lipschultz, G.M. McCracken, J. Goetz, "Scaling of Plasma Parameters in the SOL and Divertor for Alcator C-mod", in Proceedings of 11th

Int. Conf. on Plasma Surface Interactions in Controlled Fusion Devices, Mito, 1994, to be published in J. Nucl. Mat. (1994).

[10] I.H. Hutchinson, "Thermal Front Analysis of Detached Divertors and Marfes", submitted to Nucl. Fusion (1994).

[11] J. Kesner and J.P. Freidberg, "Marfe Formation in Diverted Tokamaks", MIT Report PFC/JA-94-6 (1994), to be published in Nuc Fusion.

Table I - Solutions as $p'(0)$ varies. L=12 m, $L_x = 2$ m, $n_{imp} = 1 \times 10^{18}\ m^{-3}$ and at the symmetry point $p(s = 12m) = 480$ Pa. Radiation from Eq. (3b) with $n_{imp} = 1 \times 10^{18}\ m^{-3}$.

	I	II	III	IV
$p'(0)$ (Pa/m)	0	640	1600	3200
n_N (m^{-3})	0	3.1×10^{17}	1.2×10^{19}	4.9×10^{19}
p_0 (Pa)	480	288	61	46
p_1/p_0	1	1.7	7.8	10.3
$T(0)$ (eV)	0.1	0.33	3.8	8.3
$T(L)$ (eV)	40.6	38.8	38.8	38.9
Δ (m)	0.19	0.30	0.26	0.14
$q_{\|\|}^{\dagger}$ (MW/m^2)	11	11	8.2	9.1

† parallel heat flux: $q_{\|\|} = e\gamma_s n_0 T_0^{3/2}\sqrt{2e/m_i}$ with $\gamma_s \sim 7$.

Figure Captions:

FIG. 1. Temperature vs field line length (m) for three values of upstream pressure in the constant pressure approximation: a) $p_1 = 192$ Pa solid curve, b) p_1 =480 Pa, c) $p_1 = 510$ Pa (short-dashed curve).

FIG. 2. Solution for the perturbation of the equilibrium temperature, $\delta\xi$, with γ values of 0 and -15 respectively. The equilibrium ($p_1 = 480$ Pa) is shown in Fig 1.

FIG. 3. Along-the-field-line profiles in the vicinity of the end plate for cases II (dashed curves) and III (solid curves) in Table I, i.e. for low and high neutral density: a)Temperature (eV), b)Pressure (Pa), c) Electron density (m^{-3}) and d) Radiated power loss (W/m^3).

FIG. 4. Ratio of upstream pressure to pressure at the divertor plate as a function of the neutral atomic hydrogen density (m^{-3}).

FIG. 5. Position of the ionization front (Δ) where T$\sim$10 eV point vs neutral density.

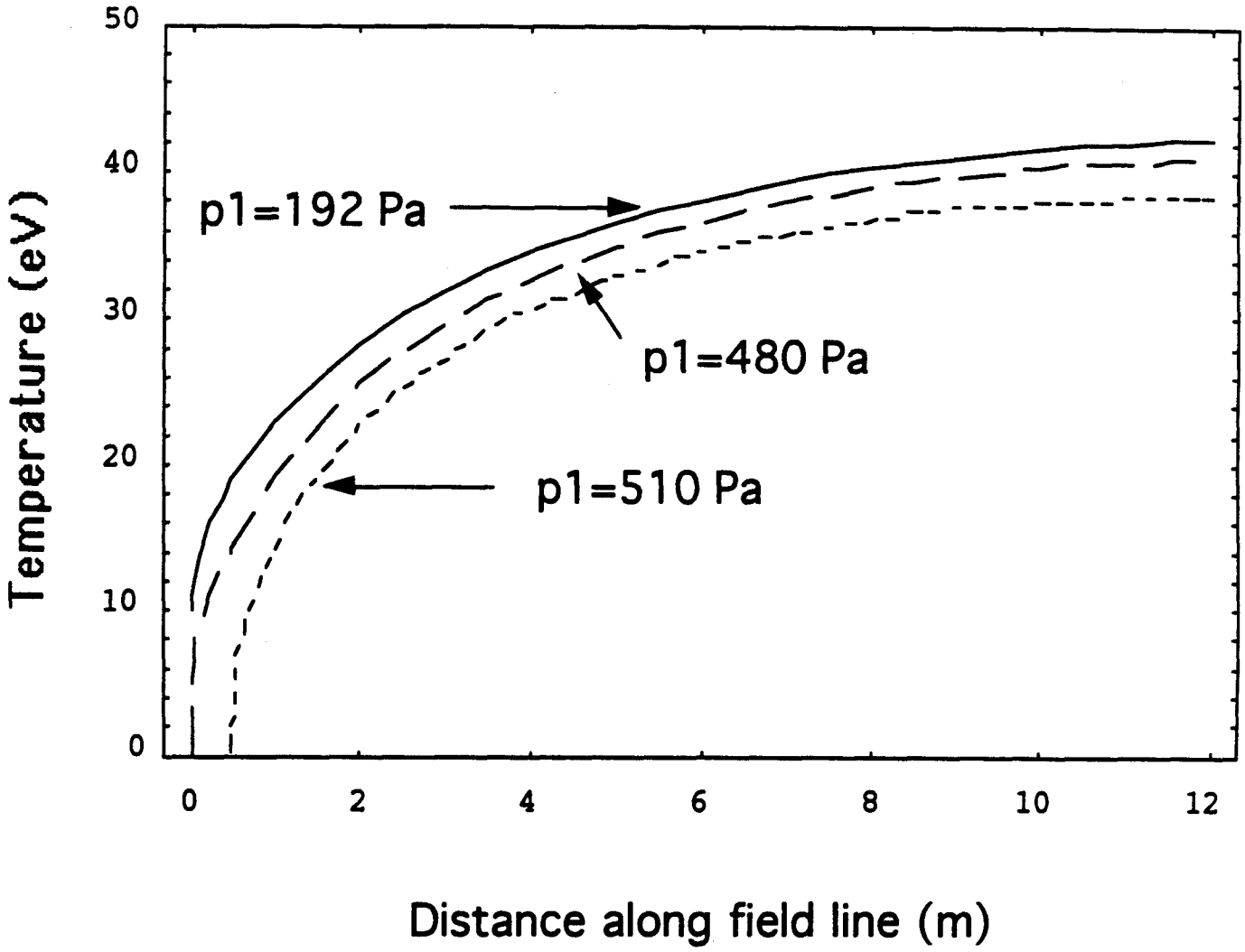

Fig 1, Kesner, PoP-20764

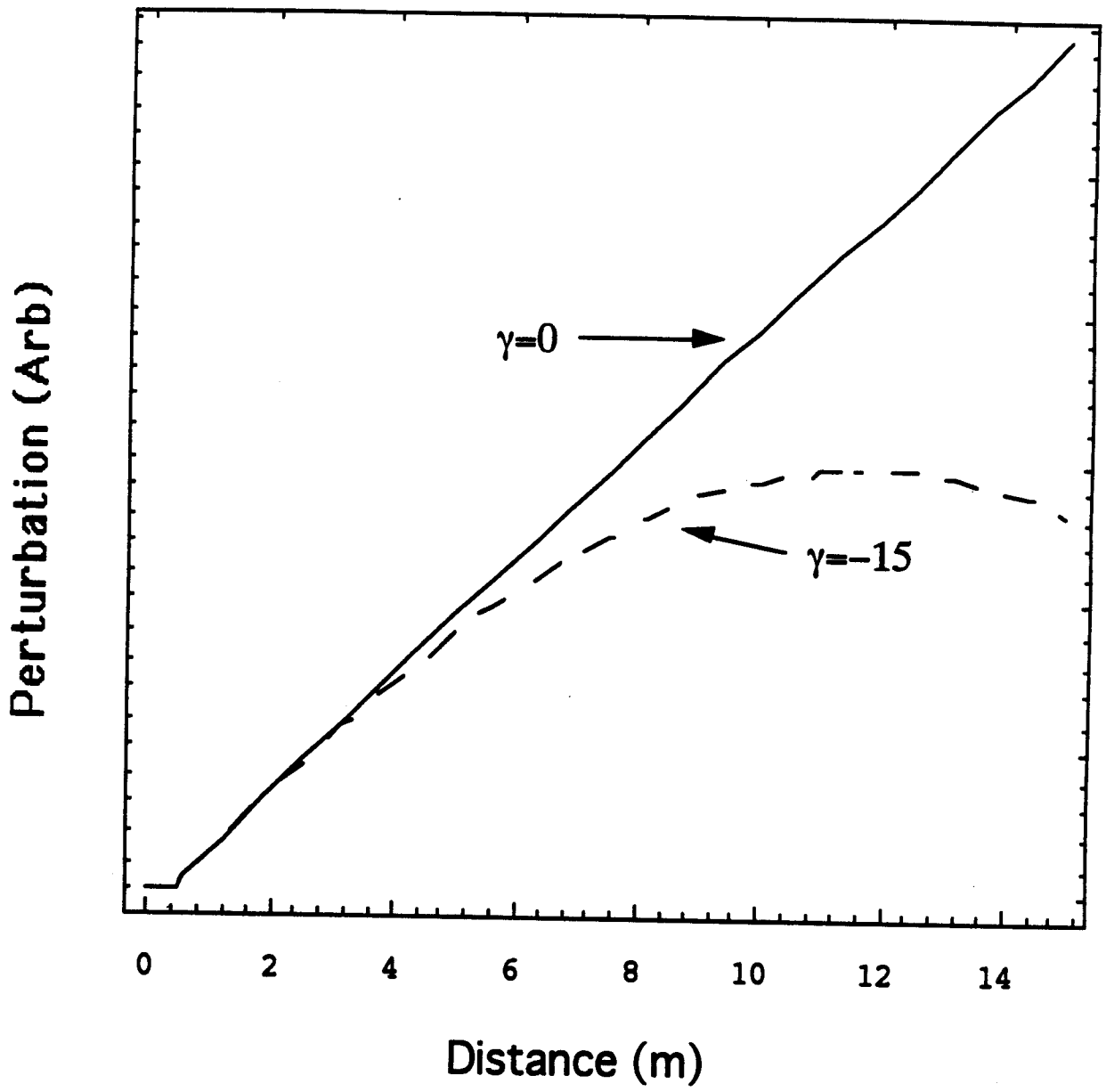

Fig 2 Kesner PoP-20764

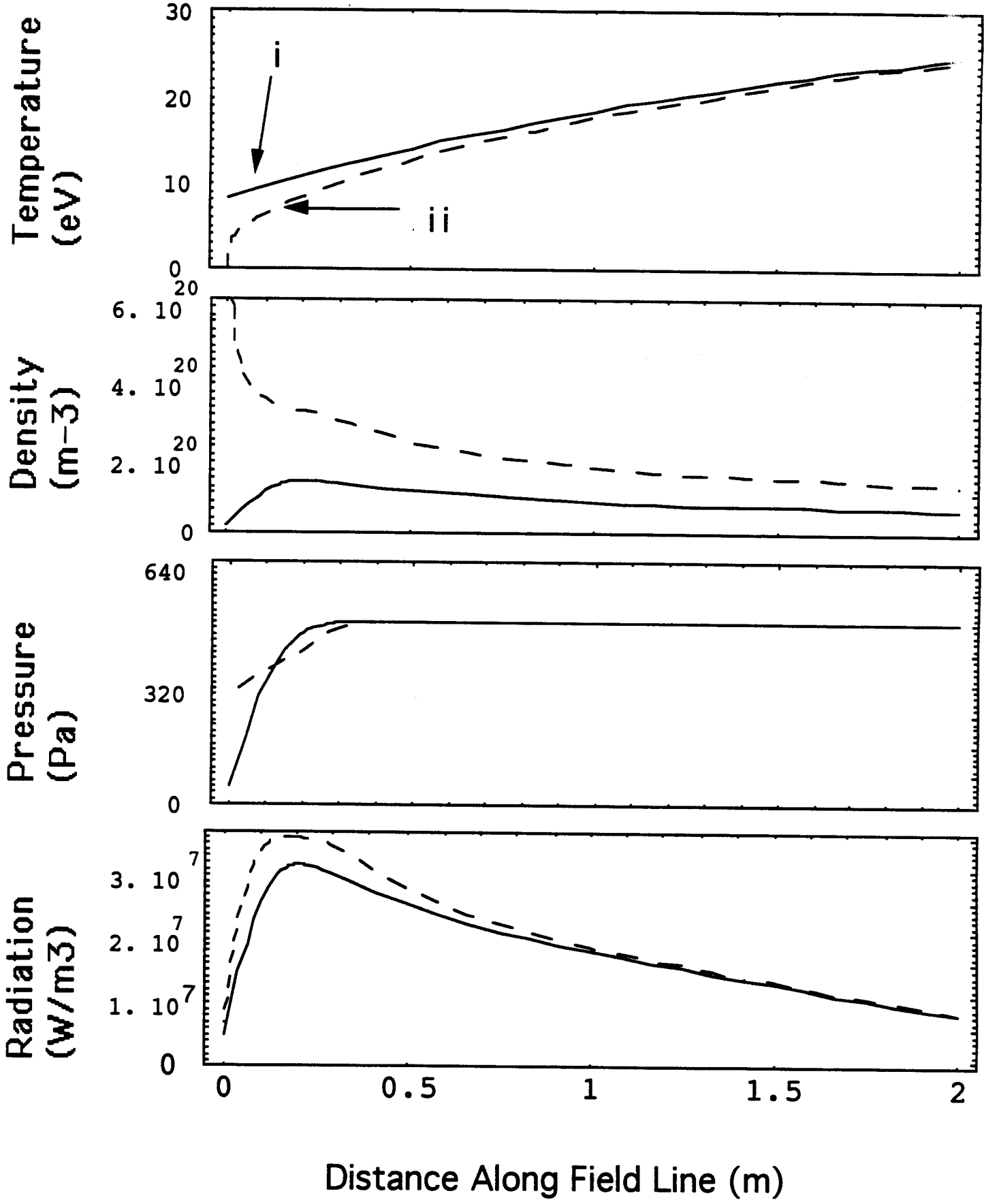

Fig 3, Kesner PoP-20764

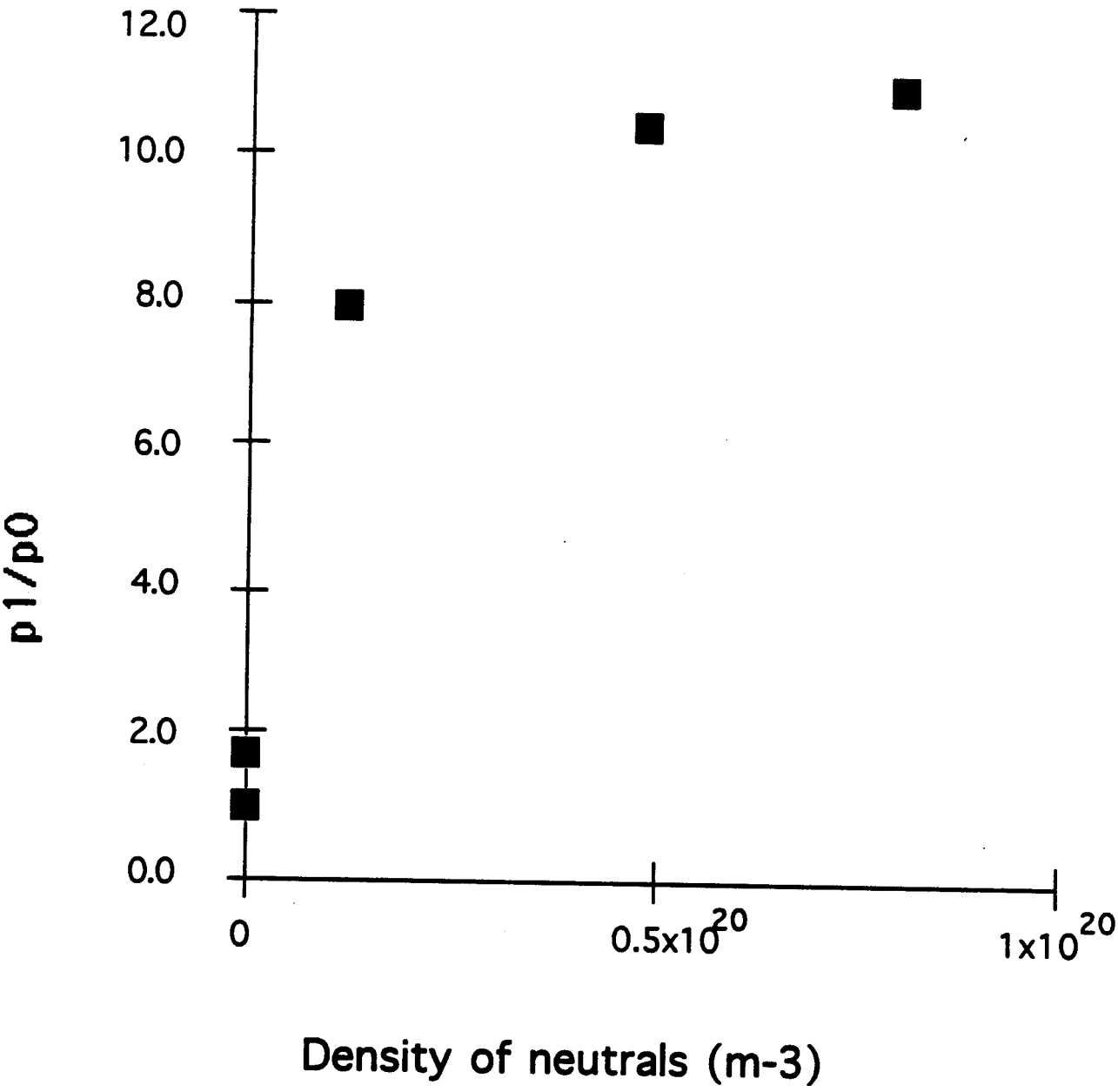

Fig 4. Kesner PoP-20764

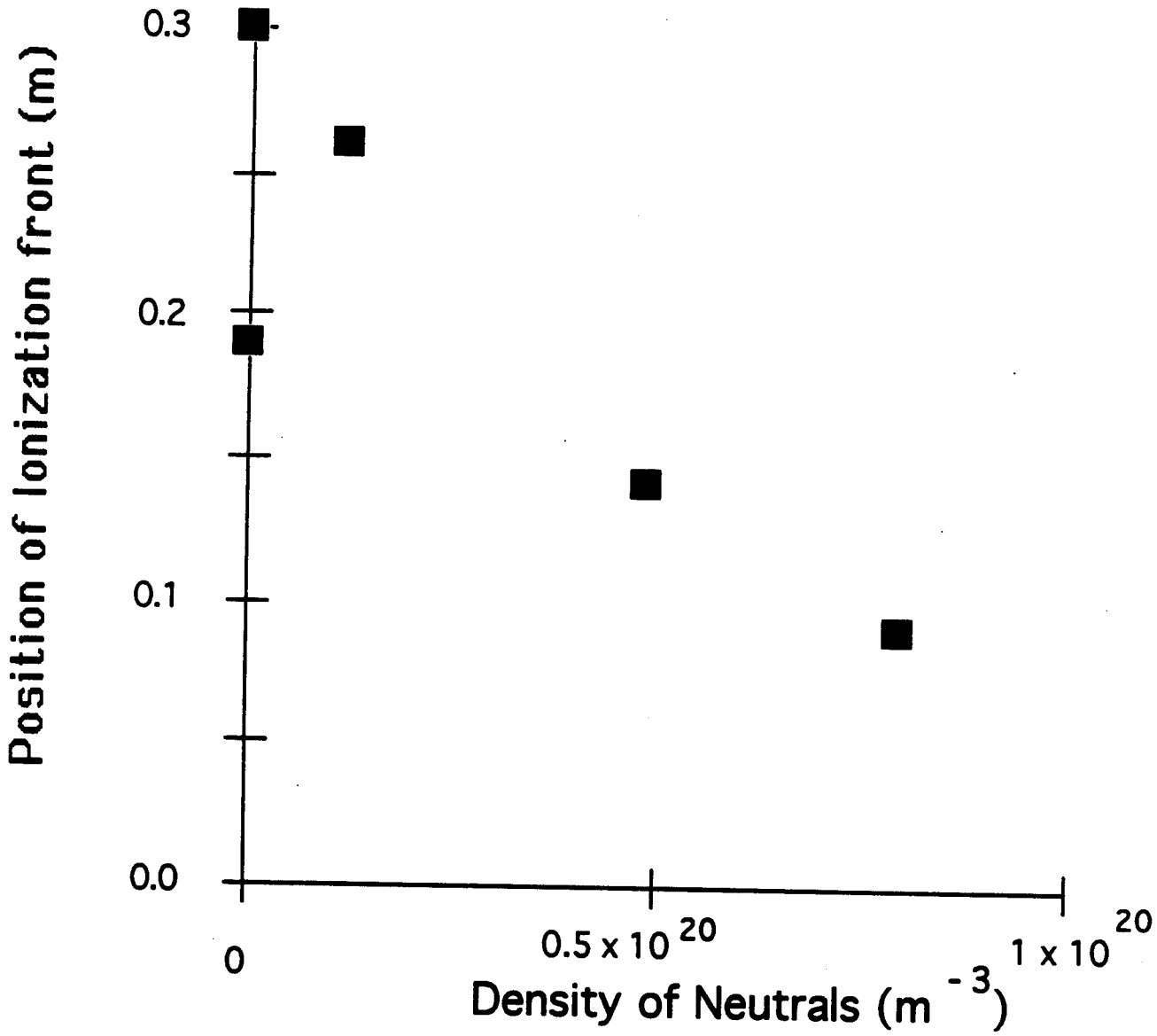

Fig 5 kesner PoP-20764